Vibrational relaxation and geminate recombination in the femtosecond-photodissociation of triiodide in solution

Thomas Kühne and Peter Vöhringer

Citation: The Journal of Chemical Physics **105**, 10788 (1996); doi: 10.1063/1.472887
View online: http://dx.doi.org/10.1063/1.472887
View Table of Contents: http://scitation.aip.org/content/aip/journal/jcp/105/24?ver=pdfcov
Published by the AIP Publishing

Vibrational relaxation and geminate recombination in the femtosecond-photodissociation of triiodide in solution

Thomas Kühne
Max-Planck-Institut für Biophysikalische Chemie, Am Faßberg, D-37077 Göttingen, Germany

Peter Vöhringer[a)]
Max-Planck-Institut für Biophysikalische Chemie, Am Faßberg, D-37077 Göttingen, Germany
and Universität Karlsruhe, Institut für Physik. Chemie, Kaiserstr. 12, D-76128 Karlsruhe, Germany

(Received 29 July 1996; accepted 19 September 1996)

The dynamics of product vibrational deactivation and subsequent geminate recombination of diiodide ions with atomic iodine following 400-nm photolysis of triiodide in ethanol solution has been studied using femtosecond transient absorption spectroscopy. The excess vibrational energy of the diatomic product was found to decay on two distinct time scales. An ultrafast subpicosecond component, which accounts for the dissipation of most of the energy that is initially deposited into fragment vibrations, is followed by thermalization near the bottom of the I_2^- potential on a time scale of several picoseconds. The former process is associated with recoil of the fragments in the exit channel of the potential energy surface relevant to bond breakage whereas the latter process represents relaxation in the asymptotic limit where interaction between the atom–diatom fragments becomes negligible. Transient product vibrational distributions are determined for delay times larger than the dephasing time of nuclear coherences in the diiodide product ions, thereby providing new information about the mechanism for bond fission. These product distributions are translated into energy-time profiles which are analyzed by a master-equation approach using various model functions for the power spectrum of solvent forces acting on the I_2^- vibrational coordinate. The dynamics of geminate recombination are found to exhibit a strongly nonexponential character and are interpreted with a simple diffusion model that takes the initial stages of bond breakage and recoil of the fragments into account. © *1996 American Institute of Physics.* [S0021-9606(96)00748-9]

I. INTRODUCTION

Elucidation of solute–solvent interactions are of primary importance in understanding chemical dynamics in condensed media. Specifically, the description of energy and momentum exchange of the reactive species with its surrounding bath plays a pivotal role in classical theories of chemical reactions occurring in the gas phase and in the liquid phase.[1–4] Relaxation of excess energy within the manifold of vibrational states of reactants and products and its time dependence in comparison to internal energy flow into and out of the reactive coordinate determine essential aspects of the reaction from overall rates and quantum yields to the nature of the reaction path. In solution phase chemistry, energy disposal to the bath may be understood tentatively as an extension of gas phase isolated binary collisions to liquid phase densities, thereby describing the dynamics of vibrational relaxation through quantities such as mean vibrational energy, $\langle E(t)\rangle$, of the nonrelaxed ensemble and average vibrational energies, $\langle \Delta E\rangle$, transferred per isolated binary collision.[4] Experimentally determined energy transfer rates, $\langle \Delta E\rangle Z$ where Z represents the binary collision frequency, may then be compared with trajectory calculations of an excited oscillator colliding with a solvent molecule. However, due to the complex nature of the solute–solvent interaction potentials, the definition of an effective collision frequency, specifically at condensed phase densities, is a difficult and sometimes arbitrary issue.

In time-dependent perturbation theory, the dissipative force that promotes relaxation of vibrational energy is generally described through its correlation function which is related to the friction exerted by the bath on the solute vibrational coordinate of interest.[5–8] The experimental as well as theoretical extraction of the associated spectral density (i.e., the Fourier transform of the corresponding correlation function of the underlying inter- and intramolecular solvent fluctuations that may couple to relaxing coordinates) is one of the most challenging topics in solution-phase chemistry.[9–14] Molecular dynamics simulations have been extremely helpful in the past in exploring solute–solvent interaction mechanisms as well as time scales involved in the process of energy dissipation. There is now overwhelming evidence from both theoretical and experimental studies that the overall rate for energy disposal into the bath is substantially enhanced by long-range Coulombic interactions between the relaxing chromophore and the solvent molecules.[11,12,15–19]

Molecular iodine in nonpolar solvents represents the most extensively studied system for vibrational relaxation in liquids. Here, the energy transfer is dominated by short-range Lennard-Jones forces and shows typical time constants ranging from several tens to hundreds of picoseconds.[20] Harris and co-workers have demonstrated the importance of isolated binary collisions in the vibrational energy transfer of I_2, after photodissociation and recombination, in a variety of solvents as well as compressed supercritical fluids.[21,22] Conceptually equivalent experiments have been conducted by Barbara and co-workers on the corresponding charged spe-

[a)]Author to whom correspondence should be addressed.

cies I_2^- in polar solvents.[16–18] Vibrational relaxation after photodissociation/recombination of diiodide exhibits relaxation rates that are more than an order of magnitude larger than in I_2, emphasizing the dramatic influence of long-range forces on the energy transfer dynamics in solution. Furthermore, the highly nonexponential behavior of the energy dissipation, specifically at high excitation energies, was attributed to a solvent-induced charge flow as evidenced by a comparison with corresponding MD simulations.[18,23]

Recent advances in time-domain spectroscopy have enabled spectroscopists to capture chemical processes in condensed media directly on the time scale of the fastest elementary step.[24–28] In particular, the generation of optical laser pulses with a duration of a few tens of femtoseconds allows for a coherent broadband excitation with preparation and detection of vibrational superposition states. The time evolution of these vibrational wavepackets in both the ground and electronically excited state offer a unique insight into details of the reaction coordinate, product state distributions and degree of coherence that is preserved during the chemical transformation and possibly transferred into the products.

In this spirit, Ruhman and co-workers have studied the photodissociation of triiodide in ethanol solution with femtosecond excitation at 308 nm.[25,26] They demonstrated that diiodide product ions emerge within 300 fs after photolysis and are vibrating coherently due to the process of impulsive photoexcitation. This coherent transfer of nuclear motion from the initial Franck–Condon region of the reactants to the products is accompanied by considerable vibrational excitation of the diatomic fragment with excess energies as great as 17 quanta. This energy was found to dissipate on a time scale of approximately 4 ps, again significantly faster than for nonpolar solutes. In similar experiments, Pugliano *et al.* have examined the relaxation dynamics of vibrationally excited HgI following the femtosecond photodissociation of HgI_2.[29–31] The polar HgI molecule is also formed in a vibrational superposition state and dephases with a time constant of 1 ps. As is the case for I_2^-, the initial excess energy of the diatomic product decays extremely rapidly on a time scale of a few picoseconds in ethanol solutions.

In this paper, additional detailed information will be presented about the dynamics and mechanisms involved in the photodissociation of I_3^- in liquid solution using excitation wavelengths centered around 400 nm. Femtosecond time-resolved pump-probe experiments are used to characterize the dynamics and time scales associated with loss of vibrational energy and geminate recombination of the fragments through reconstruction of instantaneous absorption spectra and transient vibrational product distributions. Following some experimental details, spectroscopic information about the species that participate in the dissociation reaction will be presented along with some computational details relevant to the reconstruction of transient spectra. The experimental results presented in Sec. III will be discussed extensively with respect to the various elementary chemical steps that compete in the triiodide photochemistry.

II. EXPERIMENT

The fs transient absorption spectrometer used in these experiments is based on an entirely home-built Ti:Sapphire laser/regenerative amplifier system which will be described in detail elsewhere.[32] Briefly, a Kerr-lens modelocked Ti:Sapphire oscillator is pumped by the output of a cw argon ion laser operating on all lines. The design of the x-folded cavity is similar to that described by Asaki *et al.*[33] A pump power of 5 W routinely yields a train of 15-fs duration pulses centered at 800 nm with a repetition rate at 85 MHz and 700 mW average power using a 10% output coupler at the nondispersive end of the resonator. The pulses are temporally broadened by a factor of 1000 in a diffractive pulse stretcher similar in design to that reported in Ref. 34. After passing a thin film polarizer/Faraday rotator combination followed by mode matching optics, the pulses are coupled into the linear cavity of a regenerative amplifier, which is pumped by 8 W of the 532-nm output of an acousto-optically Q-switched, intracavity frequency-doubled Nd:YAG laser. Seeding and dumping of the RGA cavity is achieved by a thin-film polarizer in combination with a Pockels cell (Medox) which is referenced to the pulse train of the oscillator. The output of the amplifier consists of optical pulses centered at 800 nm with energies of 1.5 mJ at a repetition rate of 1 kHz. The amplified pulses are recompressed in a standard double grating configuration to a duration of 30 fs, limited by the gain profile of the regenerative amplifier. The overall throughput of the compressor is 65% yielding pulse energies of approximately 1 mJ.

The photolysis pulses are obtained by frequency doubling a portion of the amplified pulses in a type-I BBO crystal with a thickness of 100 μm. The resulting pulses with a center wavelength of 400 nm had a duration of 30 fs as determined by impulsive stimulated scattering in pure water. To obtain probe pulses tunable from 400 to 1000 nm, less than one μJ of the fundamental pulses is focused into a sapphire substrate with a thickness of 1 mm. The emerging single-filament white-light continuum has a Gaussian beam profile with excellent pulse-to-pulse stability and can be used without any further amplification. Both pump and probe pulses are fed into a standard pump-probe interferometer and are spatially and temporally overlapped at the position of the sample with all-reflective optics ($f=0.5$ m) to avoid pulse broadening due to group velocity dispersion. Spectral selection is achieved using 10- to 20-nm bandwidth interference filters placed in the beam path of the probe pulse behind the sample cell. Triiodide solutions with a concentration of 3 mM were prepared as described in Ref. 16 and were circulated through a flow cell with an optical path length of 100 μm. The 400-nm pump energies were always kept below 1 μJ to avoid saturation effects.

III. RESULTS

A. Background

The static absorption spectrum of triiodide in ethanol is displayed in Fig. 1. It consists of two broad and structureless

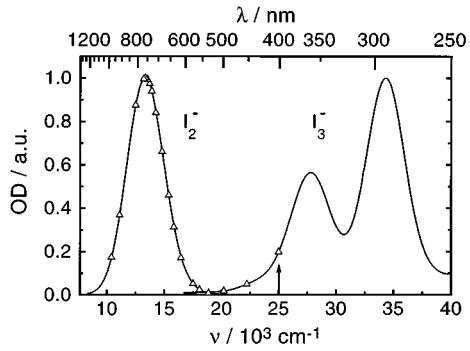

FIG. 1. Electronic absorption spectrum of triiodide in liquid ethanol. Also shown is a calculated absorption spectrum of the diiodide photofragment according to Eqs. (1)–(9). The open triangles and the vertical arrow indicate probe and pump wavelengths, respectively.

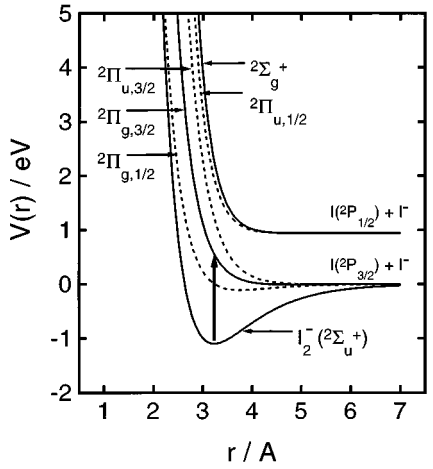

FIG. 2. Potential energy surfaces of diiodide according to Ref. 38. The vertical arrow indicates the transition that gives rise to the absorption band in the near IR.

features whose assignment is controversial. The excited electronic states associated with both bands are dissociative in nature leading to diiodide ions and atomic iodine reaction products. The ground state of I_3^- correlates with ground state molecular iodine $I_2(^1\Sigma_g)$ and iodide ions $I^-(^1S)$. Both transition dipoles are polarized along the long axis of the I_3^--molecule.[35] Tasker has given assignments for the two absorptions bands based on simple MO arguments in which the first excited state of triiodide has $^1\Sigma_u$ symmetry correlating with dissociation products $I_2^-(^2\Sigma_u)$ and $I(^2P_{1/2})$. The next excited state has Π_u symmetry and dissociates into $I_2^-(^2\Pi_g)$ and iodine radicals in their spin-orbit ground-state $^2P_{3/2}$. The energy splitting in the I_3^--absorption spectrum is thus comparable to the energy gap between the ground and excited states of diiodide reduced by the spin-orbit splitting of atomic iodine.[36] Although this assignment has been refined,[35,37] it seems clear that excitation into the low-frequency resonance gives rise to ground-state diiodide radicals. The excitation wavelength of 400 nm used in these experiments is located at the red edge of the low energy absorption band, as indicated by the vertical arrow in Fig. 1. Therefore, contributions from excited states of diiodide should only be of minor importance for the observed dynamics of triiodide photodissociation.

Also shown in Fig. 1 is a calculated absorption spectrum of the diiodide product. Although diiodide is known to have a multitude of mostly dissociative states, it was assumed that this spectrum is purely determined by the $^2\Pi_g \leftarrow ^2\Sigma_u$ resonance[38] (see Fig. 2). Potential energy surfaces reported by Chen and Wentworth[38] were used to calculate this spectrum. The electronic ground state was represented by a Morse potential

$$V_g(r) = D\ \exp[-2a(r-r_0)] - 2D\ \exp[-a(r-r_0)] \tag{1}$$

with a dissociation energy of 0.9 eV and $a = 1.31\ \text{Å}^{-1}$. This yields a harmonic frequency of 115 cm^{-1} and an anharmonicity of $\omega_e x_e = 0.49$. The $^2\Pi_g$ potential is written as an exponential

$$V_e(r) = B\ \exp\left(-\frac{r-r_0}{A}\right), \tag{2}$$

with $B = 0.72$ eV and $A = 0.33$ Å. Similar to Refs. 16 and 26, these quantities were slightly adjusted to obtain a reasonable fit to the experimental absorption spectrum reported in the literature. To calculate Franck–Condon factors, the ''reflection principle'' was used for each individual eigenstate, $|v\rangle$, in the electronic ground state.[39] Assuming the transition moments to be r independent and neglecting electronic dephasing entirely, the absorption spectrum can then be expressed for any given incoherent vibrational distribution $P(v)$ as a weighted superposition

$$I(\omega) \propto \omega \sum_{v=0}^{\infty} P(v) |\Psi(v,r)|^2. \tag{3}$$

For a given eigenvalue E_v and a given optical transition frequency ω, the wave function $\Psi(v,r)$ has be calculated at the internuclear separation r for which the resonance condition $\hbar\omega = V_e(r) - E_v$ is fulfilled, i.e., the excited-state potential enters Eq. (3) through the distance r.

For the spectrum shown in Fig. 1, a Boltzmann distribution at $T = 298$ K was used for $P(v)$. The ground state wave functions were calculated using the following analytic recursion expression:[40]

$$\Psi(v,r) = \Psi(v-1,r)\ \frac{k}{z(r)} \cdot \frac{k-2v+z(r)-(k-2v)R'(v-1,r)}{2(k-v)-(k-2v)R(v-1)}, \tag{4}$$

with

$$\Psi(0,r) = \left(\frac{z(r)}{k}\right)^{(k-1)/2} \exp\left(-\frac{z(r)-k}{2}\right). \tag{5}$$

The functions $R(v)$ and $R'(v,r)$ are defined as

$$R(v) = \frac{k-v}{v+1} \cdot \frac{-2vR(v-1)-(k-2v)}{(k-2v)R(v-1)-2(k-v)} \tag{6}$$

and

$$R'(v,r)=\frac{k-v}{v+1}\cdot\frac{(k-2v-z(r))R'(v-1,r)-(k-2v)}{(k-2v)R'(v-1,r)-(k-2v+z(r))} \tag{7}$$

and were used to eliminate Laguerre polynomials which are difficult to handle especially for large v. For $v=0$, $R(v)$ becomes zero and $R'(v,r)=k-z(r)$. $z(r)$ is expressed as $z(r)=k\exp(-\alpha(r-r_0))$ with k being related to the parameters of the Morse potential

$$k=\frac{4\pi}{ah}\sqrt{2\mu D} \tag{8}$$

and h representing Planck's constant. Referring to Fig. 1, the experimental absorption spectrum at room temperature peaks around 740 nm and has a full width at half maximum of more than 3500 cm^{-1}. This spectrum and a corresponding low-temperature spectrum compare very well with experimental data reported in the literature.[41,42] The white light continuum probe pulse covers almost the entire spectrum in the NIR and extends far into the near UV. Probe wavelengths used in these studies are indicated in Fig. 1 by open triangles. Finally, it should be noted that diiodide exhibits an additional higher lying state that gives rise to an absorption in the near UV (see Fig. 2).[38] This transition can contribute to the data in the region of the fundamental around 400 nm.

Little is known about the global potential energy surface correlating triiodide ions $^1\Sigma_u$ with diiodide radicals in $^2\Sigma_u$ and iodine atoms (^2P). Only Tasker attempted to gain insight into one dimensional surfaces along the symmetric stretching coordinate using valence bond calculations with pseudopotentials replacing atomic cores.[36] Of more relevance to this work is an empirical LEPS surface reported by Benjamin *et al.*, which was optimized by fitting the experimental absorption spectrum of I_3^- using MD trajectory calculations.[19] Johnson and Myers have modified this surface by incorporating an empirical skewing function to account for the broken symmetry that is spectroscopically evident in the presence of a solvent environment.[43,44] Using these data, it follows that excitation of the $^1\Sigma_u$ state at 400 nm yields 1.3 eV excess energy with respect to the asymptotic reaction channel. This energy can potentially be distributed among the various degrees of freedom of the fragments that are created through the process of bond fission.

B. Long-time dynamics

The probe wavelength dependence of the transient absorption following 400-nm excitation of triiodide in liquid ethanol solution is summarized in Fig. 3. For clarity, each individual transient has been arbitrarily normalized to its absorbance at 1.5 ps. The temporal behavior of the signals is extremely complex, particularly in the region close to the center of the diiodide absorption spectrum. Around zero delay time, each signal exhibits a sharp initial peak whose rise is determined by the response function of the laser system and whose decay can be described appropriately with time constants ranging from 50 to 200 fs. Subsequently, a fast rise

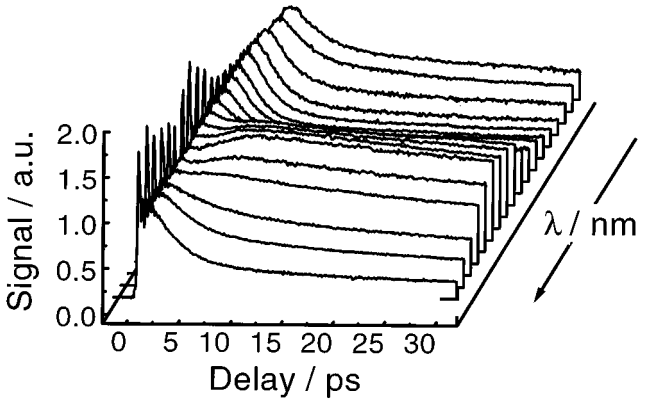

FIG. 3. Experimental pump-probe signals at various probe wavelengths. For clarity, each individual transient was arbitrarily normalized to its absorbance at 1.5 ps. The probe wavelengths are (from top to bottom): 450, 500, 530, 550, 570, 600, 630, 650, 680, 700, 720, 740, 750, 780, 810, 850, 910, and 960 nm.

can be observed at all probe wavelengths with superimposed oscillatory modulations. Due to insufficient sampling in the long time scans these oscillations are not clearly resolved but are the focus of short time transients reported in the next subsection. The rise becomes ever slower as the probe pulse is tuned further to the blue. This is evident by the shift of the first broad maximum of the signal toward longer delays as the probe wavelength approaches the absorption spectrum of triiodide. At 450 nm, the transient absorption peaks at 6 ps whereas in the near IR the signal reaches a maximum at 1.5 ps. Around 740 nm, this time-dependent increase in absorbance is followed by a slightly slower decay with small amplitude which is complete after approximately 3 to 4 ps. As the probe wavelength is further detuned from the I_2^- resonance the amplitude of this component decreases. Ultimately, the signal decays on a much longer time scale with a lifetime of more than 100 ps. An accurate decay constant for this component is difficult to specify since the signal has not decayed to a constant absorbance even at the longest delays. This behavior results in a highly nonexponential decay at the red and the blue edges of the diiodide absorption spectrum.

The contribution of the long time decay to the overall signal is also strongly dependent upon the probe wavelength; its amplitude decreases toward the edges of the steady-state spectrum of I_2^-. Further to the blue, the slow decay becomes more pronounced again, however, it should be mentioned that the absolute intensity of the signal is decreasing. Even further into the near UV with degenerate pump and probe pulses at 400 nm, the sign of the overall signal changes, thereby reflecting a transient bleach/stimulated emission component that dominates the observed dynamics. This bleach recovers within the first 5 ps, leaving a very small residual transient absorption at longer delays (see Fig. 4).

For well-separated pump and probe pulses, the signal in the region of $^2\Pi\leftarrow{}^2\Sigma$ transition of diiodide may simply be expressed as the delay-dependent overlap of the evolving diiodide absorption spectrum $I(\tau,\omega)$ with the spectrum of the probe pulse transmitted by the interference filter. Referring to $T(\omega)$ as the filter function, the signal is then given by

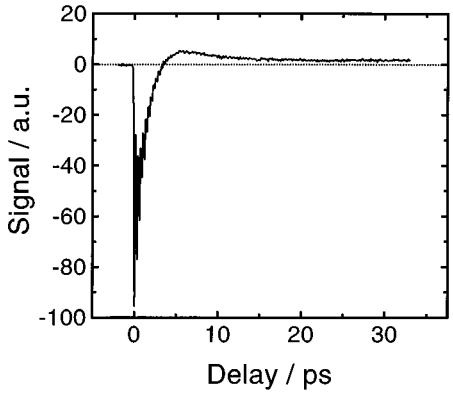

FIG. 4. Experimental signal with 400-nm pump and probe pulses. The signal shows a rapidly decaying transient bleach at short delays and a residual transient absorption on longer time scales. The sharp peaks superimposed on the bleach component correspond to incompletely resolved ground-state nuclear coherences (see also Fig. 8).

$$S(\tau,\omega)=\int_{-\infty}^{\infty} d\omega I(\tau,\omega)T(\omega), \tag{9}$$

where τ is determined by the pump-probe time delay. For most probe wavelengths, $T(\omega)$ was usually well represented by a sinc-function of appropriate width and center frequency. Equation (9) together with Eq. (3) directly connects the time resolved measurements reported in this paper to the transient vibrational distribution function of ground state diiodide after 400-nm photolysis of I_3^-. These distribution functions will be discussed later in Sec. IV. Finally, the probe-frequency integrated spectrum is a measure of the total concentration of I_2^- molecules at a given pump-probe time-delay, hence, information about cage escape and recombination can easily be obtained.

C. Short-time dynamics

Banin and Ruhman were able to demonstrate that the photolysis of I_3^- at 308 nm, i.e., with excitation into the red edge of the high-energy absorption band, results in an efficient transfer of nuclear coherence from the initially prepared Franck–Condon state into the exit channels leading to diiodide ions and atomic iodine.[25–27] This coherence originates from the process of impulsive photoexcitation of the parent molecule and is possible only if sufficiently short optical pulses are used and the reaction is also complete on a time scale less than the product vibrational period. The coherently vibrating diiodide photofragment was characterized by a vibrational dephasing time of T_2=400 fs.

In order to be able to extract information about transient vibrational product distributions in the aforementioned manner, it is of importance to precisely establish the degree of coherence or, equivalently, the dephasing dynamics that might contribute to the observed fs transients reported here. An analysis described in the previous section can only be performed for delay times ascertained to be longer than the decay time associated with the loss of vibrational coherence in the products. A full account of the vibrational wave-

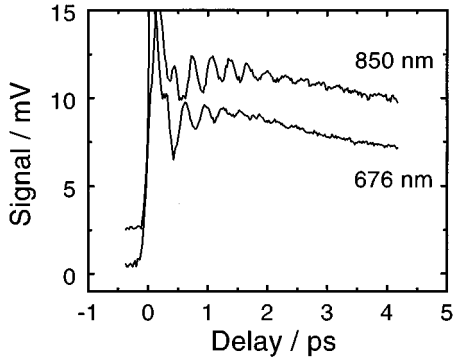

FIG. 5. Comparison of experimental fs transients demonstrating the out-of-phase behavior of the nuclear coherence at the opposite edges of the diiodide absorption spectrum.

packet dynamics will be given elsewhere,[45] however, a few points need to be mentioned before questions regarding transient vibrational product distributions can be addressed.

Two representative short time scans are displayed in Fig. 5. These data were taken at 650 and 850 nm, i.e., at the high- and low-energy side of the steady-state absorption spectrum of the product. In agreement with the results reported in Ref. 25, the oscillatory modulations have a frequency close to the harmonic frequency of diiodide. For a simple bound-to-free transition as is the case for I_2^-, a blue probe wavelength will preferentially probe the wave packet at the inner turning point of the potential along the I_2^- coordinate, whereas a redder wavelength is more sensitive to displacements corresponding to the outer turning point. Located at the opposite edges of the resonance, the data shown in Fig. 5 therefore oscillate out of phase with respect to each other. The phase angles and frequencies of the vibrational wave packet as a function of probe wavelength are shown in Fig. 6. The phase angle is increasing monotonically with probe frequency and displays a difference of π roughly at the inflection points of the I_2^- absorption (i.e., at 650 and 850 nm).

The dependence of the beat frequency on probe energy is rather unexpected. Initially, ω increases as the probe wavelength approaches the I_2^- spectrum from the low energy tail. However, as the probe frequency sweeps through the reso-

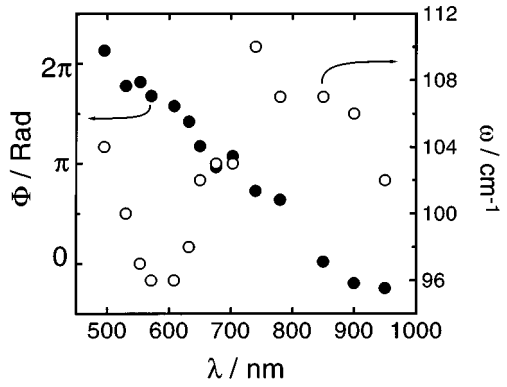

FIG. 6. Probe-wavelength dependence of the phase angle and the beat frequency of the nuclear coherences observed in the diiodide NIR resonance.

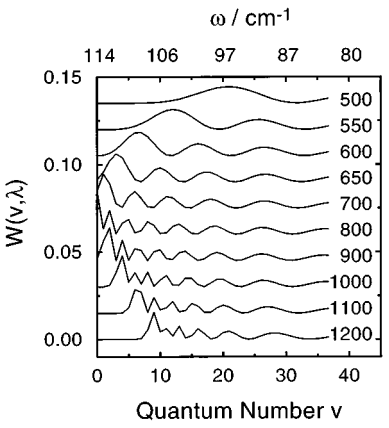

FIG. 7. Contribution of each individual vibrational eigenstate of diiodide to the absorbance at various probe wavelengths. This corresponds to a spectral window function similar to that defined in Ref. 29.

nance the beat frequency starts decreasing until it reaches a minimum around 580 nm. Further to the blue, the beat frequency increases again, presumably due to contributions from triiodide absorptions that become more important at shorter wavelengths (cf. Fig. 1). Referring to Eq. (1), the contribution of each individual eigenstate of ground state I_2^- to the total absorption can be evaluated at any given wavelength. This demonstrates indeed that the probe pulse is sensitive to vibrational states with increasing quantum number as the detuning to either side of the absorption maximum increases. The resultant mapping of the vibrational quantum number onto the probe pulse wavelengths is illustrated in Fig. 7 and can be understood as a spectral window function $W(v,\lambda)$ similar to that defined in Ref. 31.

Figure 7 indicates that probe wavelengths around 600 nm are especially sensitive to vibrational states around $v=8$ and $v=16$, which should give rise to quantum beat frequencies around 110 and 101 cm^{-1}. In contrast, the experimentally observed wave packet period in the 600-nm transient implies that much higher quantum states around $v=20$ are preferentially detected. This might suggest that the wave packet is probed at rather small interfragment separations, where the potential energy surfaces involved in the optical transition are slightly different along the diiodide coordinate compared to those given by Eqs. (1) and (2). By this reasoning, the initial 1.5 ps rise of the transient absorption in the visible can be attributed to the recoil dynamics in the exit channel, and therefore, to an increasing population of diiodide fragments in the asymptotic limit. Here, the ground and excited state surfaces reduce to the Morse and exponential potentials for isolated diiodide ions as given by Eqs. (1) and (2). In any case, the wave packet frequencies observed with 400-nm excitation indicate substantial vibrational excitation of the diatomic fragment.

As will be shown in more detail in a separate article, the experimentally observed time constants for damping of nuclear coherences are strongly probe wavelength dependent.[45] Nevertheless, an upper limit of 1 ps^{-1} can be specified. Despite this relatively fast dephasing, transient vibrational distribution functions from incoherent spectra are difficult to obtain even for delays longer than T_2. Meaningful results can only be expected after the system has finally reached the asymptotic limit. The corresponding delay can be estimated from the first maximum that is observed in the fs transients and is roughly 1.5 ps.

D. Ground-state dynamics

Further information about the initial dynamics of the wave packet on the excited state potential comes from resonance Raman experiments conducted in the frequency domain by Kiefer and Bernstein[46] and by Johnson and Myers.[43] A long progression in the symmetric stretching coordinate was observed indicating a rapid evolution of the system toward three-body dissociation. This is supported by quantum-dynamical calculations performed by Banin *et al.*[26] and Ashskenazi *et al.*[47] using the empirical LEPS surface for the linear configuration of I_3^- from Ref. 19. From preresonance Raman experiments,[43] it can further be concluded that the symmetry is considerably broken by the solvent environment as is the case for I_3^- color centers in CsI crystals.[48]

In this section, a brief report on the pump-probe data with degenerate frequencies is given. These types of experiments are known to yield complementary information to those from resonance Raman spectra. A typical signal is shown in Fig. 8 with a positive signal now indicating a transient bleach/stimulated emission. The response is dominated by strong oscillatory modulations superimposed on an overall bleach similar to those described in Sec. III C. The bleach builds up very rapidly and appears to be recovered after 4 ps. The long time scan shown in Fig. 4, however, exposes a residual transient absorption on a much longer time scale as already mentioned in Sec. III B.

An analysis using linear prediction-singular value decomposition (LP-SVD) reveals several components whose frequencies, amplitudes, phase angles, and damping constants are listed in Table I. The zero-frequency component that decays with a sub-100-fs time constant coincides with the initial peak seen in the visible/NIR region and may therefore be attributed to a transient absorption from the initial Franck–Condon state as suggested previously by Banin *et al.*[27] The components with time constants of 2 and 4 ps are presumably absorptive in nature and compare well with the transient signal observed around 500 nm. One might therefore be tempted to assign these features to product absorptions, arising from the $^2\Sigma_g \leftarrow {}^2\Sigma_u$ transition of I_2^-. However, admixtures from I_3^--transitions should not be excluded in these considerations. In fact, a fast component has also been observed in the UV with excitation wavelengths around 308 nm and was attributed to hot transitions from vibrationally excited I_3^- parent molecules being regenerated through the process of geminate recombination.[27] As will be shown later, recombination is highly nonexponential and can be determined most reliably from spectroscopic data in the NIR.

To check for consistency, a Fourier analysis of the raw data after subtraction of the slowly varying background was also performed. The corresponding spectrum is shown in the

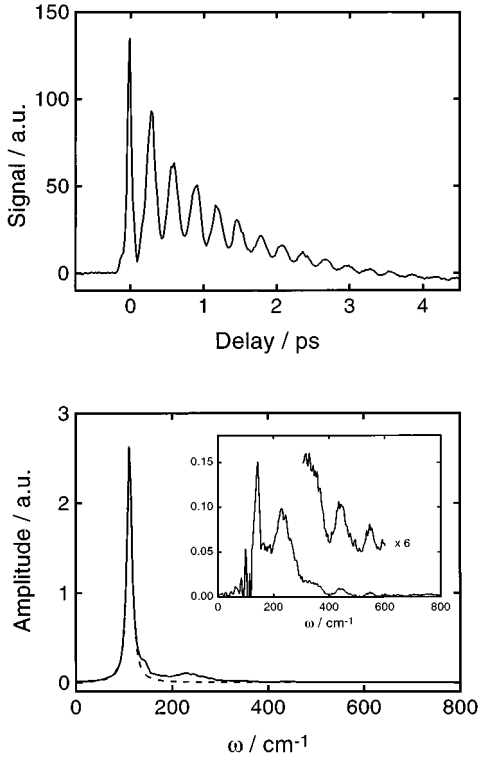

FIG. 8. Transient resonant impulsive stimulated Raman scattering of triiodide. Upper panel: experimental fs transient dominated by a ground-state vibrational coherence in the symmetric stretching coordinate. Lower panel: Fourier transform of the time domain transient after subtraction of the slowly varying background. The dashed curve represents a Lorentzian fit to the 112-cm^{-1} component. The inset shows a difference spectrum with the Lorentzian removed.

lower panel of Fig. 8. In agreement with the results from the LP-SVD analysis, the major contribution to the signal stems from an oscillation with a frequency of 111 cm^{-1}. As has been extensively discussed by Ruhman and co-workers, this component is due to a nuclear coherence in the ground state being prepared and detected through resonant impulsive stimulated Raman scattering (RISRS).[27,49] The beat frequency agrees very well with the fundamental of the symmetric stretching vibration of ground-state triiodide. Fitting this peak to a Lorentzian line shape yields a damping constant identical to that obtained from LP-SVD. Furthermore, a pronounced shoulder can be observed in the high frequency tail of the 111 cm^{-1} peak, which becomes more evident after subtraction of the dominant Lorentzian component. The difference spectrum is reproduced in the inset of Fig. 8(b) and emphasizes finer details carried in the oscillatory part of the RISRS transient. Due to the large bandwidth of the 30-fs, 400-nm pulses, higher-order quantum coherences are generated and can be distinguished from the noise up to frequencies of about 600 cm^{-1}. Most importantly, the shoulder in the high-frequency tail of the symmetric stretch now appears as a pronounced peak located at 140 cm^{-1}. The frequency agrees very well with the antisymmetric stretching vibration of I_3^- known from frequency-domain preresonance Raman studies[43] and confirms the small oscillatory component revealed by the LP-SVD analysis.

TABLE I. Linear prediction singular value analysis of the RISRS transient shown in Fig. 8.

Amplitude/a.u.	Frequency/cm^{-1}	Time constant/ps	Phase angle/deg
124	0	2.10	0
60.1	0	3.72	180
118	0	0.04	180
23.6	111	0.84	7
2.16	140	0.84	0
10.2	223	0.21	−12

IV. DISCUSSION

A. Spectral reconstruction and transient vibrational product distributions

As described earlier, the long time transients allow for a reconstruction of instantaneous absorption spectra of incoherent ensembles of diiodide radicals following 400-nm photolysis of triiodide. The underlying vibrational distribution functions, $P(v)$, were obtained at each delay independently by implementing Eqs. (1)–(9) into a least-squares fitting routine. Since there is an infinite number of vibrational states that can potentially be populated, the probability for the fitting algorithm to converge is very small. Instead, $P(v)$ has been crudely estimated by prefitting the absorption spectra manually prior to running a full least-squares analysis. It turns out that only those vibrational states contribute to the spectra which have a quantum number smaller than 15. The least-squares fitting algorithm was therefore restricted to vibrational states with $v<20$. Furthermore, the peak quantum number obtained from the prefit was fixed and various functional forms for $P(v)$ such as Gaussians or exponentials were assumed for the high- and low-energy tails. Shifting the peak of $P(v)$ by only one quantum and allowing the algorithm to reoptimize the fitting parameters usually generated fits of dramatically poorer quality or resulted in a convergence failure of the least-squares routine.

The results of this procedure are shown in Fig. 9 for four representative time delays after the population has reached the asymptotic limit. Simulated spectra are displayed as solid lines along with their corresponding distribution functions. At the earliest delays for which an accurate spectrum can be determined, the distribution peaks around $v=1, 2$ with a long exponentially decaying, high energy tail. For comparison, an absorption spectrum that results from a Gaussian distribution with the same width and center quantum number is also shown at a delay of 1.5 ps. This demonstrates the high sensitivity of the transient spectrum to finer details of the distribution function, specifically for an ensemble close to the bottom of the potential well.

As time evolves, $P(v)$ narrows and its maximum shifts toward $v=0$ while the exponential tail at high quantum numbers is more or less preserved. After 7 ps, the distribution starts to resemble a Boltzmann distribution at room temperature. The most important aspect, however, is that even at the shortest delays a significant fraction of the molecules are

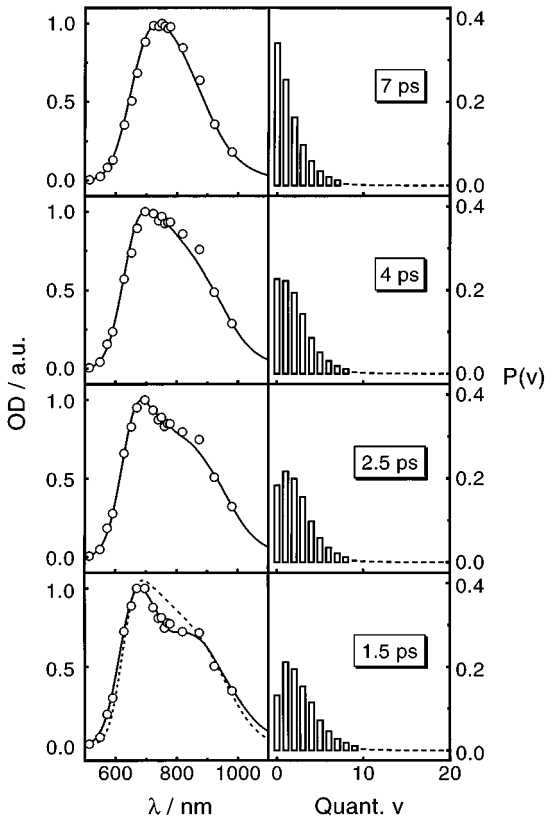

FIG. 9. Reconstructed instantaneous absorption spectra and transient vibrational distribution functions of diiodide at various pump-probe time delays. Open circles: experimental data, solid curves: calculated spectra. The dashed curve corresponds to a spectrum that results from a Gaussian distribution centered at $v=1$ with a full width at half maximum of five vibrational states.

already in their ground vibronic level. It is instructive to compare the earliest product distribution with the nuclear coherence that was observed for even shorter delay times. The wavepacket was characterized by beat frequencies between 96 and 110 cm^{-1}. If one assumes that the wave packet has already arrived at the asymptotic limit within the dephasing time T_2 one can at least estimate the initial vibrational excitation of the products. With the known anharmonicities of the I_2^- potential one calculates an average quantum number of $v=14$ which corresponds to a significantly higher degree of vibrational excitation than suggested by the incoherent spectrum measured only a few hundred femtoseconds later.

Given the lack of information about the potential energy surfaces specifically at smaller interfragment separations, these findings imply that even at the initial stages of the dissociation the solvent plays an essential role in partitioning available excess energy into the vibrational and translational degrees of freedom of the products. To reiterate, approximately 1.3 eV of excess energy is available to these modes but at very early times only a minor fraction appears as vibrational excitation as deduced from quantum beat frequencies. After dephasing is complete, the vibrational excess energy is even lower as determined from incoherent transient spectra measured only a few hundred femtoseconds later.

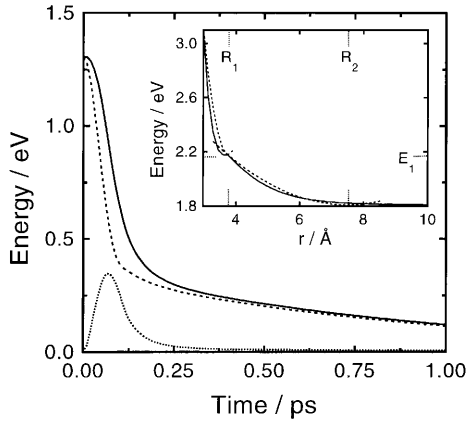

FIG. 10. Time-dependent energies of the damped oscillator model [Eqs. (13) and (14)]. Solid: total energy, dashed: potential energy, and dotted curve: kinetic energy. The inset displays a cross section through the empirical LEPS surface from Benjamin *et al.* along the direction of steepest descent together with the piecewise harmonic model potential (dashed).

This suggests that most of the energy delivered by the excitation photon is dissipated very efficiently during the early time evolution of the wave packet into the exit channels and also during its passage toward the asymptotic limit for dissociation. Therefore, one could come to the conclusion that a significant contribution to dephasing of the nuclear coherence originates from population relaxation and that the finally incoherent ensemble reaches the asymptotic limit while moving along the bottom of the exit channel toward larger interfragment separations. However, the importance of anharmonicities along the I_2^- coordinate for vibronic dephasing needs to be mentioned here and was clearly demonstrated through quantum dynamical simulations by G. Ashkenazi *et al.*[47]

To estimate the energy dissipated during the recoil of the fragments in a viscous fluid, knowledge about the potential energy surface along the reaction path is necessary. The inset in Fig. 10 shows a cross section of the empirical LEPS surface from Benjamin *et al.* along the direction of steepest descent.[19] This surface can be approximated by piecewise harmonic potentials referenced to the Franck–Condon point of initial excitation ($r=2.98$ Å)

$$V_i(r)=\tfrac{1}{2}k_i(r-R_i)^2+E_i\,. \tag{10}$$

For $r<R_1$, the force constant is given by

$$k_1=2\,\frac{E_0-E_1}{R_1^2}, \tag{11}$$

where E_0 is determined by the excess energy of the excitation photon with respect to the asymptotic limit, in the present case $E_0=1.3$ eV. R_1 and E_1 correspond to the location and the energy of the saddle point on the LEPS surface, respectively. Here, R_1 equals (3.76–2.98) Å, and $E_1=0.37$ eV. For $R_1<r<R_2$, the force constant is switched

$$k_2=2\,\frac{E_1}{(R_1-R_2)^2}. \tag{12}$$

R_2 is adjusted to yield a reasonable fit of the model potential to the LEPS surface. With $R_2=(7.5–2.98)$ Å, one obtains the dashed curve shown in Fig. 10. The equation of motion that governs the dynamics on the model potential can then be written as

$$\mu_i\ddot{x}+b\dot{x}+k_i x=0, \tag{13}$$

with $x=r-R_1$ for $r<R_1$ and $x=r-R_2$ for $r>R_1$. Here, μ_i denotes the appropriate reduced mass. During the recoil, the fragments are subject to a frictional force of Stokes' type $F=6\pi\eta a v$, where a and v are the hydrodynamic radius and the velocity of the fragments, respectively. η represents the viscosity of the solvent and is 1 cP for ethanol at room temperature. Further, it is assumed that the radius is identical for both fragments. From the Lennard-Jones diameter of iodine radicals one can estimate a value of $a=2.15$ Å. To calculate the energy dissipation due to friction during the recoil of the fragments, it is assumed that the diatomic fragment has no internal degree of freedom. It then follows that

$$b=3\pi a\eta. \tag{14}$$

Equation (14) describes the motion of a damped oscillator whose energy is plotted as a function of time in Fig. 10. In agreement with the experimental observations, considerable energy dissipation takes place on an ultrashort time scale well below half a picosecond. As suggested above, after 0.5 ps the system tends to move along the bottom of the potential. In light of this certainly oversimplified calculation, it is not surprising that vibrational excitation in the diiodide product is rather small. Of particular interest is the kinetic energy of the system at displacements that correspond to the location of the saddle point. One finds

$$E_1=\frac{1}{2}\,k_1R_1^2\,\exp\left\{-\frac{b}{2\mu_1\Omega_1}\left[\arctan\left(-\frac{2\mu_1\Omega_1}{b}\right)+\pi\right]\right\}, \tag{15}$$

where the effective frequency Ω_1 is given by

$$\Omega_1=\sqrt{\frac{k_1}{\mu_1}+\left(\frac{b}{2\mu_1}\right)^2}. \tag{16}$$

This yields a value of 0.18 eV. Together with the saddle point energy of 0.37 eV, one finds a total energy of 0.55 eV that could potentially be deposited into fragment vibrations at infinite product separations. From the beat frequencies observed in the short time transients, an average vibrational excitation of 0.19 eV was derived. This value agrees surprisingly well with the kinetic energy calculated at the saddle point.

From these findings, it is tempting to draw the following simple picture for energy loss during the early stages of bond breakage. As already known from resonance Raman experiments and quantum dynamical simulations, initial acceleration occurs along the symmetric stretch. However, this motion is efficiently hindered by solvent friction resulting in substantial energy dissipation within the first 120 fs. Once the system has reached the saddle point, it is reflected into the exit channel where the remaining kinetic energy is effectively converted into product vibrational excitation. The frictional drag on the fragments that continue to separate toward the asymptotic limit forces the system to propagate along the bottom of the potential. The system ultimately reaches the asymptotic limit but not before dissipating almost the entire excess energy that remained available at the saddle point.

Again, it must be pointed out that the above calculations represent only a rough estimate of the energetics that accompany the dynamics of product separation in a viscous medium. Clearly, the above description of the solvent environment as a hydrodynamic continuum with a frequency-independent friction coefficient is questionable especially in light of the ultrashort nature of time scales and frequencies involved in the processes of bond breakage as well as decay of energy and coherence observed in the diatomic product. A more realistic, molecular-level description of the dynamics of vibrational thermalization for delays larger than the vibrational dephasing time will be given later.

Nevertheless, it is illustrative to compare these very simple model calculations and the experimental results presented in this paper to more elaborate molecular dynamics simulations performed by Benjamin *et al.*[19] Their calculations show that most of the energy that can be deposited into the fragments is transferred within the first 100 fs. During this time the translational energy of the I_2^- product reaches its maximum value of 0.3 eV. These findings agree very well with the kinetic energy displayed in Fig. 10. As was pointed out in Ref. 19, the vibrational energy of the diatomic molecule is difficult to specify unless the interaction between the products becomes negligible. The molecular dynamics simulations indicate an initial vibrational excitation of about 4 kcal/mole corresponding to 0.17 eV in very good agreement with both the experimental value obtained from the quantum beat frequencies and with the conclusions drawn from the simple model calculations reported above. Furthermore, at 1.5 ps the MD simulations imply a residual vibrational excess energy of 0.08 eV. From the earliest transient product distributions one can calculate a mean vibrational energy of about 0.04 eV (see below) which is half the value obtained from MD simulations. Therefore, the time constant for vibrational relaxation of 1.3 ps that was specified by Benjamin *et al.* should be regarded as an upper limit. The results presented here suggest a time constant similar to the dephasing time of the vibrational coherence. As will be shown later, however, relaxation of excess vibrational energy of diiodide after photodissociation of I_3^- appears to be strongly biexponential.

B. Recombination dynamics

The transient vibrational product distributions reported in the previous section were normalized at each delay to a total probability of unity. However, to reproduce the instantaneous absorption spectra accurately, a level-independent scaling parameter was needed to account for diiodide molecules that geminately recombine and, hence, do not contribute to the wavelength-integrated absorbance. The delay-dependent scaling parameter was determined for each delay, thereby providing information about the probability of cage

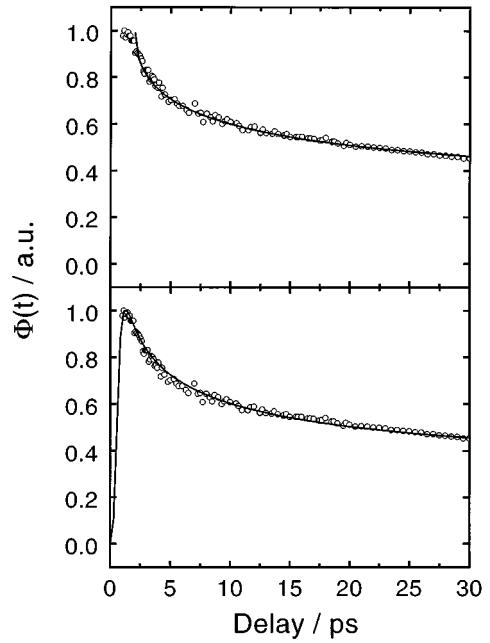

FIG. 11. Time-dependent quantum yield for triiodide photodissociation. Open circles: experimental data, upper panel: simple diffusion model [Eq. (18)], lower panel: $\Phi(t)$ from diffusion model convoluted with a time-dependent flux of products at the contact distance R.

break out or, equivalently, the quantum yield, $\Phi(t)$, for photodissociation. The fraction of nonrecombined diiodide radicals as a function of pump-probe time delay is shown in Fig. 11. A closer inspection of these data reveals that the recombination dynamics are highly nonexponential. A fit to a simple double-exponential decay yields time constants of 2.45 and 73 ps with corresponding amplitudes of 0.26 and 0.66, respectively.

In the following, these results will be discussed in the context of a simple diffusion model for geminate recombination that was developed by Troe and co-workers[50] from the original work by Noyes.[51] This model has been applied very successfully in representing experimental data for the primary recombination of iodine atoms formed through photolysis of molecular iodine in compressed gases and liquids.[50] The analysis is based on solving an ordinary diffusion equation which describes the evolution of a distribution $n(r,t)$ of recombining fragments with respect to time t and interfragment separation r

$$\frac{\partial n(r,t)}{\partial t} = D\,\frac{\partial^2 n(r,t)}{\partial r^2}. \tag{17}$$

Proper boundary conditions, termed the ''radiation boundary condition,'' are necessary at the contact distance, R_c, defining the largest possible separation of the fragments that still allows for the process of recombination. Initial conditions $n(r,0)$ are specified as a delta-function located at an initial separation, r_0, from which diffusion drives the system to either recombination for configurations with $r<R_c$ or further separation (i.e., cage break out) for configurations with $r>R_c$. The parameter r_0 is defined as the distance where the initially recoiling fragments attain zero velocity. For sufficiently high viscosities, the initial separation equals the contact distance. For smaller viscosities, r_0 has to be calculated from the model potential given by Eq. (10) with $k=0$ for $r>R_2$. According to the observations made in the previous section, it is reasonable to assume that the high damping limit is valid, i.e., $r_0=R_c=R_2$. Following Otto *et al.*, one obtains for the time-dependent quantum yield of product formation[50,52]

$$\Phi(t)=1-\frac{R_c}{r_0}\left(\frac{k_g}{k_g+k_d}\right)\left\{1-\mathrm{erf}\left(\frac{r_0-R_c}{2\sqrt{Dt}}\right)-\exp[B^2Dt + B(r_0-R_c)]\left[1-\mathrm{erf}\left(B\sqrt{Dt}+\frac{r_0-R_c}{2\sqrt{Dt}}\right)\right]\right\},$$

where B is given by

$$B=\frac{1}{R}\left(\frac{k_g+k_d}{k_d}\right). \tag{19}$$

erf is the error function and $k_d=4\pi RDN_A$, where N_A is the Avogadro number. The diffusion coefficient of the recombining fragments, D, in a given solvent is hereafter approximated as the solvent self-diffusion coefficient. The gas phase recombination rate coefficient is given by k_g which for the present system is not known *a priori*.

A fit of Eq. (18) to the experimental data is presented in Fig. 11 by a dashed curve. The quantum yield, $\Phi(t)$, was however shifted along the time axis by 2 ps in order to get reasonable agreement with the data. This time shift may be thought of as an induction period associated with the motion of the wave packet along the repulsive potential that connects the Franck–Condon state with the asymptotic limit at the contact distance R_c. It should be pointed out that along with k_g this time shift is the only adjustable parameter of the model. The fit yields a value for k_g of 3.4×10^{13} $\mathrm{cm^3\,mole^{-1}\,s^{-1}}$, similar to the gas phase high-pressure rate coefficients for recombination of iodine radicals in CO_2 and n-hexane.[50]

It is important to realize that in the present system multiple, physically distinct, elementary processes have to occur prior to the actual recombination of diiodide ions with iodine radicals, and these steps may compete on similar time scales. First, following absorption of the excitation photon, the wave packet is accelerated along the interfragment separation. Next, the friction associated with the motion in the exit channel leads to considerable dispersion of translational energy of the fragments which corresponds to a broadening of the wave packet along r until it finally reaches the asymptotic limit. The transfer of momentum to the bath leads to excitation of intra- and intermolecular translational, rotational, vibrational, and librational modes in the first (few) solvent shell(s) followed by energy dissipation from the cage into the bulk. Finally, before the ground state surface can ultimately be populated, the system has to undergo a radiationless transition. Since the ground state of I_3^- correlates with molecular iodine and iodide ions (^2S), this radiationless transition may be viewed as a charge transfer process. At this stage, a com-

plete and quantitative modeling of all these aspects of the dissociation dynamics is of course beyond the scope of this paper. The above, simplified description that involves a separation of the initial stages of bond fission and recoil from the subsequent diffusion part that mimicks the actual recombination is certainly no longer valid.

The above model can be improved by convolving $\Phi(t)$ as given by Eq. (18) with the finite response of the system to an infinitely fast recombination. Basically, this amounts to calculating a time-dependent flux, $J(r_0,t)$, of particles at the contact distance, R_c, which results from the amplitude approaching the asymptotic limit. The time evolution of the corresponding probability distribution, $p(r,t)$, on the repulsive surface can be illustrated by a diffusion process in a field of force, thereby reducing the problem to solving the Smoluchowski equation with the potential function given by Eq. (10). Infinitely fast recombination is then achieved by placing a perfect pinhole sink at the contact distance. Initial conditions are again specified as a delta function for $p(r,0)$, but now, at the Franck–Condon point for excitation. The probability distribution for a single harmonic potential with a pinhole sink located at the origin has been calculated by Bagchi and is zero exactly at the sink at all times.[53] Inside the sink r_s, one obtains for the total population[53]

$$P(r_s,t)=1-\mathrm{erf}\left\{\sqrt{\frac{k/\beta}{2D[1-\exp(-2kt/\beta)]}}\right\}\exp\left(-\frac{kt}{\beta}\right), \tag{20}$$

where k is the force constant of the potential and $\beta=k_BT/D$ represents the friction coefficient. The corrected time-dependent quantum yield, $\Phi'(t)$, is then approximated as

$$\Phi'(t)\approx\int_{-\infty}^{\infty}dt'\Phi(t-t')J(r_0,t') \tag{21}$$

and $J(r_0,t)$ is proportional to the time derivative of Eq. (20). In order to make use of the above expressions, the model potential has to be modified to a single harmonic potential that represents the LEPS surface for all r. This introduces the equilibrium distance of the harmonic model potential as an additional fitting parameter, but the time shift is then no longer required. The result of these calculations is shown in Fig. 11 as the solid curve. The fit was obtained using a literature value for the diffusion coefficient of ethanol and a slightly different value of k_g than before. The gas phase high-pressure rate coefficient is now 2.9×10^{13} $\mathrm{cm}^3\,\mathrm{mole}^{-1}\,\mathrm{s}^{-1}$ and the contact distance is 5 Å. Again, with the assumption of sufficiently high damping, the initial separation was fixed and set equal to the contact distance thereby reducing this model to a two-parameter fit. The agreement between the calculation and the experimental data is very good. More importantly, the empirical time shift can now be eliminated completely from this simple diffusion model. It arises naturally from the underlying dynamics connected with motion and spreading of the wave packet during the recoil of the fragments along r. On the other hand, the contact distance has become dramatically smaller indicating that recombination already occurs when the system is located in the exit channels. This might suggests that a description of the recoil dynamics by Brownian motion in a harmonic well is inappropriate, however, it has to be emphasized that the actual process of recombination can be well represented by simple diffusion.

The ultrafast recombination at very early delay times is somewhat surprising since curve crossings between ground and excited state surfaces are not known to exist. On the other hand, the results discussed in Sec. III A imply that very strong interactions between the recoiling fragments and the surrounding cage already exist at the very early stages of the dissociation dynamics. Recombination upon a single (or a few) collision(s) with a solvent molecule could explain this very small contact distance. Additional experimental investigations in a variety of solvents and pressure-dependent studies are in progress. These efforts, in conjunction with more sophisticated Brownian dynamic simulations, will be extremely helpful in improving the current picture of the recombination dynamics and the role of the solvent played therein.

C. Vibrational relaxation

It was mentioned in Sec. III A that the transient product distributions allow for the calculation of an average vibrational energy $\langle E(t)\rangle$ of the diiodide product after it has reached the asymptotic limit. It was further concluded that most of the energy that is initially deposited into product vibrations is dissipated on an ultrashort time scale similar to the dephasing time of nuclear coherences. The earliest incoherent spectrum reveals a product distribution centered around vibrational states with extremely low quantum number. Despite this low degree of vibrational excitation, the high sensitivity of probe wavelengths in the visible to vibronic states with relatively low-quantum numbers (cf. Figs. 3 and 7) gives rise to a pronounced spectral evolution for several picoseconds. The average vibrational excess energy can therefore be determined according to

$$\langle E(t)\rangle=\frac{\Sigma_v P(v,t)E(v)}{\Sigma_v P(v)}. \tag{22}$$

The decay of vibrational excess energy is illustrated in Fig. 12. At the earliest delays, the total vibrational energy in the diatomic photofragment is extremely small and corresponds roughly to 2 kT. Within the noise of these data, the excess energy decays exponentially with a single time constant of 3.5 ps. The time constant is somewhat faster than previously reported but in agreement with experimental studies on other highly polar solutes. However, the energy decays much slower than estimated from the short time spectral evolution. To remind the reader, the quantum beat frequency implies an initial average vibrational excitation of 0.17 eV, which decays to 0.04 eV within less than a picosecond due to very strong interactions with the surrounding cage during the recoil. The subsequent spectral evolution reflects the dissipation of the remaining 0.04 eV excess energy and takes place

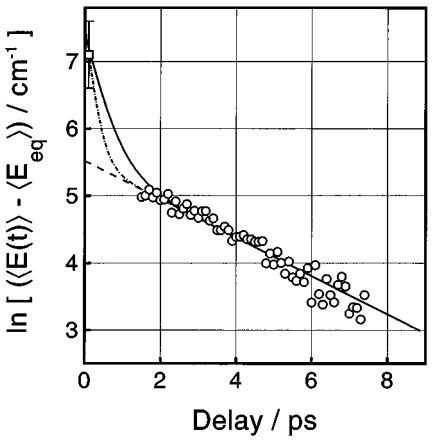

FIG. 12. Average vibrational energy of the diiodide photofragment as a function of pump-probe time delay. The dashed line corresponds to a single-exponential energy decay with a time constant of 3.5 ps. Solid curve represents a biexponential energy decay with amplitudes of 1400 and 250 cm^{-1} and time constants of 400 fs and 3.5 ps, respectively. Dotted-dashed curve: same parameters as before, but with a time constant of 200 fs for the fast component (coherent limit).

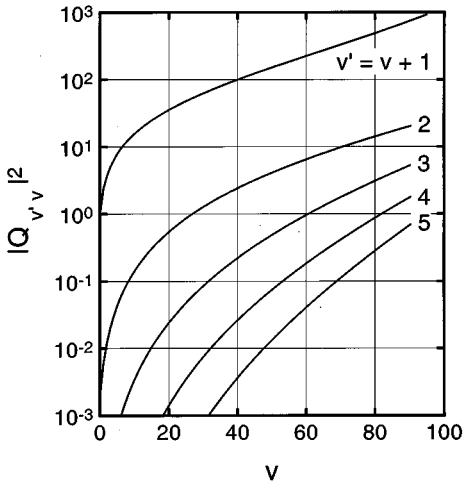

FIG. 13. Representative coupling matrix elements $|\langle v'|q|v\rangle|^2$ of the anharmonic diiodide oscillator that are off-diagonal by 1 to 5 quanta. The matrix elements are displayed in reduced units of $(2\pi\mu\omega_{10}/h)^{1/2}$.

on a time scale of about 10 ps (cf. Fig. 12). On this time scale the fragments are likely to become separated by one or a few solvent molecules.[19]

Also displayed in Fig. 12 is the average energy estimated from the quantum beat frequencies together with the time-dependent energy that results from biexponential decays. The time constants and amplitudes are given in the figure caption. The time constant of the slow component was set to 3.5 ps, while that of the fast component was (i) set to the average vibrational dephasing time observed in the short time transients (i.e., $T_1=T_2=400$ fs) and (ii) set equal to $T_2/2$ (i.e., the coherent limit is obeyed). Both cases give a reasonable fit to the experimental data. In accordance with the suggestions made in Sec. IV A, it can be concluded that population relaxation contributes significantly to dephasing of vibrational coherences in the diiodide product.

In a series of papers, Barbara and co-workers have shown that the excess energy in highly vibrationally excited diiodide generated through dissociation and recombination of diiodide itself decays in a highly nonexponential fashion.[16–18] This behavior was attributed to a solvent assisted charge-flow resulting in a much stronger internuclear distance dependence of the friction (projected onto the vibrational coordinate of relaxing I_2^-) than usually expected from molecular dynamics simulations as well as for nonpolar solutes.[18,23] The experimental data were analyzed with a master-equation approach using state-to-state rate constants which increase nonlinearly with vibrational quantum number. Instead of using empirically adjusted transition probabilities, Pugliano *et al.* used state-to-state rate constants, $k_{v\leftarrow v'}$, evaluated at the transition frequency, $\omega_{v,v'}$, from an independently determined, frequency-dependent friction, $\zeta(\omega)$, to describe the dynamics of vibrational relaxation of HgI after photodissociation of HgI_2.[30] With the assumption that the relaxing solute is bilinearly coupled to the harmonic degrees of freedom of the bath, they employed a polarizability spectral density obtained from optical Kerr-effect experiments as a measure of $\zeta(\omega_{v,v'})$, leaving the rate constant for the $1\leftarrow 0$ transition as the only adjustable parameter.

From the experimental results presented here, it seems likely that vibrational energy relaxation of diiodide following photolysis of I_3^- is highly biexponential with an ultrafast component on a subpicosecond time scale and a subsequent slower component on a time scale of several picoseconds. The former is associated with motion of the recoiling fragments in the exit channel, whereas the latter is connected with thermalization in the asymptotic limit where interaction between the fragments becomes negligible. The question that immediately arises is whether this nonexponential behavior can be explained with a single spectrum of forces acting on the I_2^- vibrational mode in ethanol solution or whether this spectrum is significantly different in these two regimes. The data displayed in Fig. 12 represent thermalization near the bottom of the potential where the anharmonicity is small. Consequently, only a narrow spectral window of the frequency-dependent friction is probed in the long-time transients and a nonexponential decay at such small excess energies cannot be expected. To explore the influence of anharmonicities in the present system in more detail, the coupling matrix elements, $|Q_{v'v}|^2=|\langle v'|Q|v\rangle|^2$, that promote transitions from v to v' $(=v+1,2,\ldots,n)$ are shown in Fig. 13. The matrix elements were calculated using the I_2^- Morse oscillator wave functions as given by Eqs. (4)–(7). As will be discussed later in this section, the individual rate constant for transitions between two vibrational states with quantum number v' and v is proportional to $|Q_{v'v}|^2$. Therefore, Fig. 13 implies that multiple quantum transitions in the energy range of interest for these experiments have negligible influence on the vibrational relaxation dynamics. Even for an ensemble starting to relax from $v=14$ as suggested by the wave packet period, multiple quantum jumps should only have a minor influence given that the friction exerted by the

bath on the anharmonic I_2^- oscillator is only a moderate function of frequency.

To be more quantitative, precise information about the state-to-state rate constants is essential. Benjamin and Whitnell have studied vibrational relaxation of diiodide in water and ethanol using molecular dynamics simulations.[15] Both solvents were found to dissipate excess energy very rapidly with typical time constants of 0.6–0.7 ps, in accordance to experimental results from Barbara and co-workers.[18] These time constants are also in semiquantitative agreement with the ultrafast component observed in the present study. Furthermore, a Landau–Teller model was found to reproduce vibrational relaxation times reasonably well.[15] According to this treatment, the power spectrum of the fluctuating force exerted on the solute was calculated at the oscillator frequency for the solute frozen at its equilibrium geometry. The importance of long-range interactions between the solvent and the solute in accelerating the rate of energy relaxation when excess charges are present has been clearly demonstrated. In addition, it was shown that the rather low frequency of the I_2^- oscillator emphasizes the role of purely Lennard-Jones-type forces, which are less efficient in relaxing excess energy in high-frequency modes such as those found in the methyl chloride system.[11,12]

Experimental estimates of the frequency-dependent friction relevant to vibrational relaxation in highly polar or charged systems may become accessible through modern femtosecond far-IR spectroscopies of the neat liquid.[54] Furthermore, measurements of the solvent response of the liquid (e.g., as detected through the THz free-induction decay) to the perturbation from a solute undergoing a chemical transformation as well as vibrational relaxation can also be envisioned in the near future. At the moment, however, one has to rely on information that stems from time-domain Raman spectroscopies such as impulsive stimulated scattering or heterodyne-detected optical Kerr-effect (OHD-OKE).[55] These techniques are sensitive to intra- and intermolecular polarizability fluctuations of the pure liquid and may therefore be inappropriate for the present system. Nevertheless, an attempt was made to model the dynamics of vibrational relaxation of I_2^- with a master-equation approach utilizing state-to-state transition probabilities obtained from the OHD-OKE response of neat ethanol. This provides an experimental comparison to recent investigations on the vibrational relaxation of HgI conducted by Pugliano *et al.*[30]

The master equation includes all possible upward and downward transitions for each individual vibrational state and is written in the form

$$[\dot{v}](t) = -\sum_{i=1}^{v} k_{v-i\leftarrow v}\cdot[v] - \sum_{i=1}^{N-v} k_{v+i\leftarrow v}\cdot[v] + \sum_{i=1}^{v} k_{v\leftarrow v-i}\cdot[v-i] + \sum_{i=1}^{N-v} k_{v\leftarrow v+i}\cdot[v+i], \tag{23}$$

where $[v]$ denotes the population in vibrational states with quantum number v. The state-to-state rate constants, $k_{v'\leftarrow v}$,

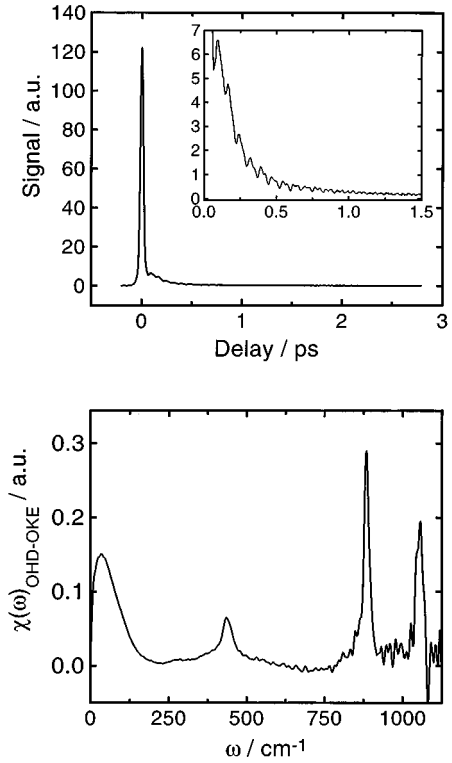

FIG. 14. Optical heterodyne-detected optical Kerr-effect of pure ethanol. Upper panel: femtosecond time-domain transient with the inset focusing on the nuclear contribution to the response. The sharp peak around zero time delay reflect the instantaneous electronic response. Lower panel: Depolarized Raman susceptibility of liquid ethanol obtained from the deconvoluted Fourier transform of the time-domain data.

obey detailed balance and are derived from the imaginary part of the depolarized Raman susceptibility as measured through the OHD-OKE response of liquid ethanol

$$k_{v'\leftarrow v} = \frac{g(\omega_{v'v})^2}{\hbar^2}\,|\langle v|Q|v'\rangle|^2\left\{1+\coth\left(\frac{\hbar\omega_{v'v}}{2kT}\right)\right\} \times \mathrm{Im}\,\chi_{\text{OHD-OKE}}(\omega_{v'v}), \tag{24}$$

where $g(\omega)$ represents the strength of the coupling of the various harmonic bath degrees of freedom that bilinearly couple to the solute anharmonic vibrational coordinate. Without explicit knowledge about the frequency and mode-dependent couplings, $g(\omega)$ has to be made an adjustable parameter which is equivalent to fitting the individual rate constant for the 0←1 transition. The coupling matrix elements $|\langle v|Q|v'\rangle|^2$ are displayed in reduced format in Fig. 13. The optical Kerr response of ethanol and the associated imaginary part of the susceptibility are displayed in Fig. 14 with the inset emphasizing the short time nuclear response that gives rise to the broad structureless band well below 250 cm^{-1} in $\mathrm{Im}[\chi(\omega)]$. These features are associated with translational, rotational, librational, and vibrational degrees of freedom of the liquid with depolarized Raman activity. The collective nature of these modes has been discussed extensively in the literature.[55,56] At higher frequencies, intramolecular Raman-active vibrations of ethanol dominate the non-

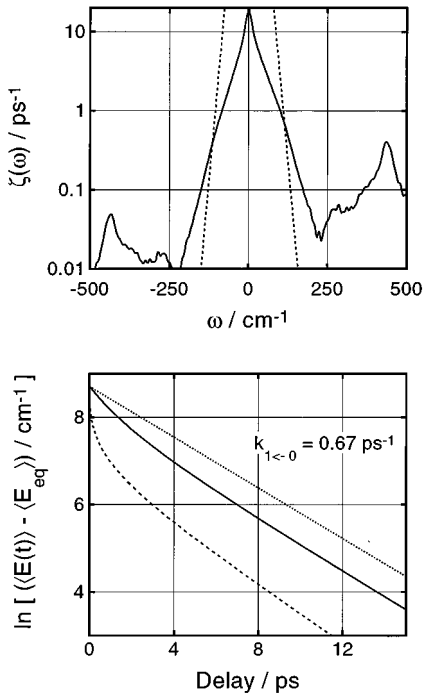

FIG. 15. Upper panel: Solvent power spectrum derived from the nonlinear susceptibility shown in Fig. 14. The dashed curve represents a model spectrum that gives rise to a significantly nonexponential energy decay of the anharmonic diiodide oscillator. Lower panel: Time-dependent vibrational energy of diiodide. Solid curve: energy decay calculated using the experimental solvent power spectrum of ethanol shown in the upper part. dashed curve: energy decay resulting from the model spectrum. Dotted curve: vibrational relaxation of the harmonic oscillator. For the anharmonic oscillator an initial vibrational distribution centered at $v=80$ with a full width at half maximum of ten vibrational states was assumed.

linear susceptibility. In the present system of a low-frequency relaxing coordinate, these intramolecular degrees of freedom may only be of importance for multiple quantum transitions which are exactly on resonance (V–V transfer as opposed to V–T transfer). The susceptibility was subsequently transformed into a solvent power spectrum using a coupling strength $g(\omega)$ that results in a state-to-state rate constant for the 1–0 transition $k_{1\leftarrow 0}$ of 0.67 ps^{-1}. The state-to-state rate constant for the $v'\leftarrow v$ transition can be calculated by multiplying $\zeta(\omega_{v'v})$ shown in Fig. 15 with the appropriate coupling matrix element $|Q_{v'v}|^2$ displayed in Fig. 13. In the case of a harmonic oscillator, these matrix elements are proportional to the quantum number and vanish for multiple quantum transitions. Thus the energy decay of a harmonic oscillator[57] having a frequency of 114 cm^{-1} is then described by a rate constant $k_{\mathrm{exp}}=k_{1\leftarrow 0}\cdot[1-\exp(-h\nu/kT)]=0.285$ ps^{-1}, where k_{exp} equals the experimentally determined energy-decay rate constant as derived from the long time part of Fig. 12. It should be noted here that $\zeta(\omega_{v'v})$ decays slightly faster with frequency than a friction spectrum obtained from MD simulations for I_2^- in ethanol and water.[15]

The energy decay that results from Eqs. (22) and (23) is illustrated in Fig. 15 along with the spectrum of solvent fluctuations derived from the susceptibility of ethanol. The initial vibrational distribution was chosen to be Gaussian, centered around $v=80$ with a full width at half maximum of ten vibrational eigenstates. As was expected, the average energy of the diiodide oscillator decays very nonexponentially. For comparison, the energy decay of a harmonic oscillator having a frequency of 114 cm^{-1} is shown by the dotted line. The nonexponential behavior observed in these calculations, however, is by far not as pronounced as the experimental data (see Fig. 12). An even more pronounced nonexponential relaxation was observed by Barbara and co-workers who studied the process with much higher initial excess energies than in the present study.[16–18] In ethanol solution, they found time constants of 24 fs and 1.1 ps, respectively, by fitting the energy profile to a biexponential decay law. In addition, they modeled state-to-state rate constants with the empirical expression $k_{v'\leftarrow v}=v\ k_{1\leftarrow 0}\exp(\alpha v)$. In such a system, the energy decay becomes noticeably nonlinear for values of α larger than 0.02. In ethanol solution a value for α of 0.2 ± 0.05 was found.

Finally, in an attempt to understand the nature of the solute/solvent interactions that give rise to such a strong nonexponential energy relaxation in I_2^-, various power spectra that satisfy the above expression were constructed by modeling the susceptibilities as ohmic line shape functions $\chi(\omega)=\omega\exp(\omega/\omega_c)$. These were subsequently translated into state-to-state rate constants according to Eq. (24) and compared with the expression given by Barbara and co-workers.[18] A solvent power spectrum that gives rise to $\alpha=0.1$ with $k_{1\leftarrow 0}=0.67$ ps^{-1} is shown in Fig. 15 as the dashed curve together with the time profile for the energy decay of an ensemble with an initial excitation of up to 80 quanta and a half width of ten vibrational states. The energy relaxes extremely nonexponential similar to the experimental data reported in Ref. 18, however, the power spectrum decays unrealistically fast. Benjamin *et al.* have attributed this nonexponentiality to solvent-assisted charge flow resulting in a internuclear distance-dependent friction.[23] The nonexponential energy decay of vibrationally excited I_2^- generated through dissociation of triiodide can equivalently be explained with an interfragment distance dependence of the friction. The ultrafast component is associated with recoil of the fragments at smaller interfragment separations in the repulsive exit channel and the 3.5-ps component is connected to thermalization in the asymptotic limit with negligible interaction of the fragments that may, furthermore, be separated by their individual solvation shells. Unfortunately, in the latter case, vibrational excitation is too small to probe the influences of anharmonicities with sufficient sensitivity. Measurements on polar as well as nonpolar molecules with much higher initial excess energy are in progress to further explore the nature of nonexponential energy decays and the associated solvent/solute interaction mechanisms.

V. SUMMARY

In conclusion, we have provided new extensive spectroscopic data on the femtosecond photodissociation of triiodide in ethanol solution. Time scales for the competing processes of vibrational relaxation in the diatomic product and gemi-

nate recombination were accurately established. This has become possible through spectral reconstruction of instantaneous absorption spectra, which allow for extraction of transient vibrational product distributions as well as the time-dependent quantum yields for diiodide product formation. The dynamics of recombination can be interpreted surprisingly well with a simple diffusion model that incorporates the early stages of bond breakage and recoil of the fragments in the exit channels. Vibrational relaxation in I_2^- appears to occur on two distinct time scales that are connected with motion of the system on the dissociative potential energy surface and thermalization in the asymptotic limit. The vibrational energy is extremely small after dephasing of nuclear coherences in the diatomic photofragment is complete. The earliest incoherent absorption spectrum revealed a population distribution centered around vibrational states with quantum numbers close to 1. At 1.5 ps, the vibrational energy in the I_2^- product is only about 2 kT, however, the high sensitivity of visible probe wavelengths to product distributions very close to the bottom of the I_2^- potential allowed for a sufficiently accurate characterization of the energy transfer dynamics on a picosecond time scale. Model calculations utilizing a master equation approach with state-to-state rate constants derived from model solvent power spectra have been performed to gain insight into the nature of the solute/solvent interactions relevant to this system. Further experiments are in progress which focus on the vibrational relaxation dynamics of more highly excited solutes to probe the influence of anharmonicities and frequency-dependent state-to-state rate constants with higher sensitivity.

ACKNOWLEDGMENTS

We gratefully acknowledge financial as well as technical support by Professor H. Hippler and Professor J. Troe. We thank Dr. D. Schwarzer for very helpful discussions and preprints of unpublished results. P.V. thanks Professor Norbert Scherer and his students for their hospitality.

[1] J. T. Yardley, *Introduction to Molecular Energy Transfer* (Academic, New York, 1980).
[2] M. Quack and J. Troe, in *Gas Kinetics and Energy Transfer*, edited by P. G. Ashmore and R. J. Donovan, Spec. Per. Rep. (The Chemical Society, London, 1977), Vol. 2, p. 175.
[3] H. Hippler and J. Troe, in *Bimolecular Reactions*, edited by M. N. R. Ashfold and J. E. Baggott, Adv. in Gas-Phase Photochem. and Kinetics (Royal Society of Chemistry, London, 1989), p. 209.
[4] J. Troe, J. Chem. Phys. **77**, 3485 (1982); J. R. Barker, J. Phys. Chem. **88**, 11 (1984).
[5] D. W. Oxtoby, Adv. Chem. Phys. **47**, 487 (1981).
[6] J. Chesnoy and G. M. Gale, Ann. Phys. Fr. **9**, 893 (1984).
[7] J. C. Owrutsky, D. Raftery, and R. M. Hochstrasser, Annu. Rev. Phys. Chem. **45**, 519 (1994).
[8] R. W. Zwanzig, Phys. Fluids **2**, 12 (1959).
[9] J. S. Bader and B. J. Berne, J. Chem. Phys. **100**, 8359 (1994).
[10] M. Tuckerman and B. J. Berne, J. Chem. Phys. **98**, 7301 (1993).
[11] R. M. Whitnell, K. R. Wilson, and J. T. Hynes, J. Phys. Chem. **94**, 8635 (1990).
[12] R. M. Whitnell, K. R. Wilson, and J. T. Hynes, J. Chem. Phys. **96**, 5354 (1992).
[13] H. Gai and G. A. Voth, J. Chem. Phys. **99**, 740 (1993).
[14] M. Bruehl and J. T. Hynes, Chem. Phys. **175**, 205 (1993).
[15] I. Benjamin and R. M. Whitnell, Chem Phys. Lett. **204**, 45 (1993).
[16] D. A. V. Kliner, J. C. Alfano, and P. F. Barbara, J. Chem. Phys. **98**, 6375 (1993).
[17] J. C. Alfano, Y. Kimura, P. K. Walhout, and P. F. Barbara, Chem. Phys. **175**, 147 (1994).
[18] P. K. Walhout, J. C. Alfano, K. A. M. Thakur, and P. F. Barbara, J. Phys. Chem. **99**, 7568 (1995).
[19] I. Benjamin, U. Banin, and S. Ruhman, J. Chem. Phys. **98**, 8337 (1993).
[20] A. L. Harris, J. K. Brown, and C. B. Harris, Annu. Rev. Phys. Chem. **39**, 341 (1988).
[21] M. E. Paige and C. B. Harris, J. Chem. Phys. **93**, 3712 (1990).
[22] A. L. Harris, M. Berg, and C. B. Harris, J. Chem. Phys. **84**, 788 (1986).
[23] I. Benjamin, P. F. Barbara, B. J. Gertner, and J. T. Hynes, J. Phys. Chem. **99**, 7558 (1995).
[24] N. F. Scherer, L. D. Ziegler, and G. R. Fleming, J. Chem. Phys. **96**, 5544 (1992).
[25] U. Banin, A. Waldman, and S. Ruhman, J. Chem. Phys. **96**, 2416 (1992).
[26] U. Banin, R. Kosloff, and S. Ruhman, Isr. J. Chem. **33**, 141 (1993).
[27] U. Banin and S. Ruhman, J. Chem. Phys. **98**, 4391 (1993).
[28] See, e.g., *Ultrafast Phenomena IX*, Springer Series in Chemical Physics, edited by G. Mourou, P. F. Barbara, A. H. Zewail, and W. H. Knox (Springer, New York, 1994).
[29] N. Pugliano, D. K. Palit, A. Z. Szarka, and R. M. Hochstrasser, J. Chem. Phys. **99**, 7273 (1993).
[30] N. Pugliano, A. Z. Szarka, S. Gnanakaran, M. Treichel, and R. M. Hochstrasser, J. Chem. Phys. **103**, 6498 (1995).
[31] N. Pugliano, A. Z. Szarka, and R. M. Hochstrasser, J. Chem. Phys. **104**, 5062 (1996).
[32] P. Vöhringer (in preparation).
[33] M. T. Asaki, C. P. Huang, D. Garvey, J. Zhou, H. C. Kapteyn, and M. M. Murnane, Opt. Lett. **18**, 977 (1993).
[34] J. Zhou, C. P. Huang, M. M. Murnane, and H. C. Kapteyn, Opt. Lett. **20**, 64 (1995).
[35] T. Okada and J. Hata, Mol. Phys. **43**, 1151 (1981).
[36] P. W. Tasker, Mol. Phys. **33**, 511 (1977).
[37] H. Isci and W. R. Mason, Inorg. Chem. **24**, 271 (1985).
[38] E. C. M. Chen and W. E. Wentworth, J. Phys. Chem. **89**, 4099 (1985).
[39] A. S. Winans and E. C. G. Stueckelberg, Proc. Natl. Acad. Sci. **14**, 867 (1928).
[40] H. Kobeissi, J. Comput. Phys. **61**, 351 (1985).
[41] P. Fornier de Violet, R. Bonneau, and J. Joussot-Dubien, Chem. Phys. Lett. **28**, 569 (1974).
[42] T. Shida, Y. Takahashi, H. Hatano, and M. Imamura, Chem. Phys. Lett. **33**, 491 (1975).
[43] A. E. Johnson and A. B. Myers, J. Chem. Phys. **102**, 3519 (1995).
[44] A. E. Johnson and A. B. Myers, J. Chem. Phys. **104**, 2497 (1996).
[45] Th. Kühne and P. Vöhringer (in preparation).
[46] W. Kiefer and H. J. Bernstein, Chem. Phys. Lett. **16**, 5 (1972).
[47] G. Ashkenazi, R. Kosloff, S. Ruhman, and H. Tal-Ezer, J. Chem. Phys. **103**, 10005 (1995).
[48] M. R. Mohammad and W. F. Sherman, J. Mol. Struct. **115**, 320 (1984).
[49] U. Banin, A. Bartana, S. Ruhman, and R. Kosloff, J. Chem. Phys. **101**, 8461 (1994).
[50] B. Otto, J. Schroeder, and J. Troe, J. Chem. Phys. **81**, 202 (1984).
[51] R. M. Noyes, Prog. React. Kinet. **1**, 131 (1961).
[52] K. Razi Naqvi, K. J. Mork, and S. Waldenstrøm, J. Phys. Chem. **84**, 1315 (1980).
[53] B. Bagchi, J. Chem. Phys. **87**, 5393 (1987).
[54] B. N. Flanders, R. A. Cheville, D. Grischkowski, and N. F. Scherer, J. Phys. Chem. **100**, 11824 (1996).
[55] P. Vöhringer and N. F. Scherer, J. Phys. Chem. **99**, 2684 (1995).
[56] See, e.g., P. Madden and D. J. Tildesley, Mol. Phys. **55**, 969 (1985).
[57] E. W. Montroll and K. E. Shuler, J. Chem. Phys. **26**, 454 (1957).